SAND2017-0747C

# Significance of RON, MON, and LTHR for Knock Limits of Compositionally Dissimilar Gasoline Fuels in a DISI Engine

**David Vuilleumier and Magnus Sjöberg**
Sandia National Laboratories



## Abstract

Spark-ignition (SI) engine efficiency is typically limited by fuel auto-ignition resistance, which is described in practice by the Research Octane Number (RON) and the Motor Octane Number (MON). The goal of this work is to assess whether fuel properties (i.e. RON, MON, and heat of vaporization) are sufficient to describe the anti-knock behavior of varying gasoline formulations in modern engines. To this end, the auto-ignition resistance of three compositionally dissimilar gasoline-like fuels with identical RON values and varying or non-varying MON values were evaluated in a modern, prototype, 12:1 compression ratio, high-swirl (by nature of intake valve deactivation), directly injected spark ignition (DISI) engine at 1400 RPM. The three gasolines are an alkylate blend (RON=98, MON=97), a blend with high aromatic content (RON=98, MON=88), and a blend of 30% ethanol by volume with a gasoline BOB (RON=98, MON=87; see Table 2 for details).

The preliminary findings of this work are that RON and MON, when coupled with latent heat of vaporization information, are sufficient to describe the auto-ignition resistance of a fuel to a degree such that knock-limited combustion phasing shows no measurable differences. While the tested fuels yielded no inconsistencies between their ratings (RON and MON) and properties (latent heat of vaporization) and their performance in a DISI engine, measurable differences were found among the three tested fuels. Specifically, the manner in which the fuels obtained knock-resistance varied, be it through thermal tolerance, charge cooling, or lack of charge-heating Low-Temperature Heat Release (LTHR). In addition, the fuels' knock-limited combustion phasing responses to variations in intake pressure and intake temperature varied with their thermal tolerance and tendency towards LTHR. Yet these dissimilar behaviors combine to produce similar anti-knock qualities and engine performance for naturally-aspirated operation.

## INTRODUCTION

Gasoline Spark-Ignition (SI) engines are the dominant form of combustion engine in the U.S. light-duty market, and have been for many decades. A significant impediment to SI engine efficiency is auto-ignition of the end-gas prior to consumption of the end-gas by deflagration-based combustion [1]. Auto-ignition of the end-gas typically produces a sharp, metallic noise referred to as knocking, and can cause problems with vehicle Noise, Vibration, and Harshness (NVH), as well as problems with premature engine failure.

Knocking is fundamentally caused by compression of the end-gas, which raises the temperature and pressure of the end-gas to the point of auto-ignition. The compression heating is due to the pressure rise caused by piston motion in combination with an expansion of the burned gases as the flame propagates. Knocking is avoided in a number of ways, which typically fall into two categories: alterations to the engine or engine operating conditions which reduce peak temperatures and pressures faced by the end-gas, or selection of a fuel that is more resistant to auto-ignition. This study focuses on understanding the resistance of different fuels to auto-ignition, in order to enable the use of more efficient operating conditions in modern SI engines.

Knocking hampers SI engine efficiency by limiting the compression ratio employed in production engines; analysis of the ideal Otto thermodynamic cycle shows the compression ratio has an important role in determining the efficiency of Otto engines, as seen in Eq. 1.

$$\eta = 1 - (1/(CR\hat{}(\gamma-1))) \qquad \text{Eq. 1}$$

By employing fuels which are more resistant to end-gas auto-ignition, SI engines can be produced and calibrated to be more efficient by making use of higher compression ratios and optimal spark timing.

This study is part of a broader research program named Co-Optimization of Fuels and Engines (Co-Optima) [2], run by the Department of Energy, whose goal is to identify opportunities that arise when fuels and engines are co-optimized. This study investigates the important hypothesis used in the Co-Optima project, namely that fuel properties are sufficient to predict the behavior of fuels in engines. An example of this hypothesis is that a fuel's RON [3], MON [4], and latent Heat of Vaporization (HoV) describe the fuel's resistance to auto-ignition in a SI engine relative to other fuels. To test this hypothesis, this study uses three carefully selected fuels, which share the same RON, but vary MON and HoV.

A significant body of work exists which relate RON and MON ratings of fuels to SI engine performance [5, 6, 7]. In particular, the Octane Index [8, 9, 10] has been shown to reasonably predict the knock resistance of fuel in engines; this method estimates knock resistance based on weighting RON and MON ratings via information specific to the engine and operating point of interest. While this method works well to an engineering approximation, it is not clear that this method works well with non-petroleum based fuels, or fuels with varying HoV's [11]. Thus, for the purpose of evaluating novel, bio-derived fuel molecules as part of the Co-Optima project

[2], a deeper understanding of the role of fuel properties and specifications on knock-resistance is desired.

This study assesses the knock-resistance and underlying phenomena of three gasoline-type fuels, which will be described in detail in the following section. It will be shown that these fuels are resistant to end-gas auto-ignition for different combinations of chemical auto-ignition resistance and charge cooling effects, yet behave similarly in the engine as would be expected by their matching RON and similar MON ratings.

## Experimental Setup

### *Research Engine Facility*

The engine used for the experiments is a single-cylinder four-valve research engine that can be set up in two configurations: an all-metal configuration for continuously fired performance testing, or in a nearly identical optical configuration for imaging studies. All tests here were conducted with the all-metal configuration, using a water-cooled metal cylinder and oil-lubricated metal piston rings, and run at an engine speed of 1400 RPM. The piston has a moderately deep piston bowl to aid the stratification of fuel for spray-guided stratified-charge operation, *e.g.* Ref. [12]. However, for these tests the fuel was injected during the intake stroke to generate a well-mixed charge. Figure 1 shows a cross section of the combustion chamber with the piston at TDC. The long-reach spark plug allows the spark plasma to develop in a central location of the combustion chamber, which should be particularly beneficial for lean operation; however, in this work only stoichiometric un-diluted conditions were tested. This long-reach spark plug is used with a high-energy inductive ignition system, as described in the "Conventional Inductive Spark System" section of this manuscript.

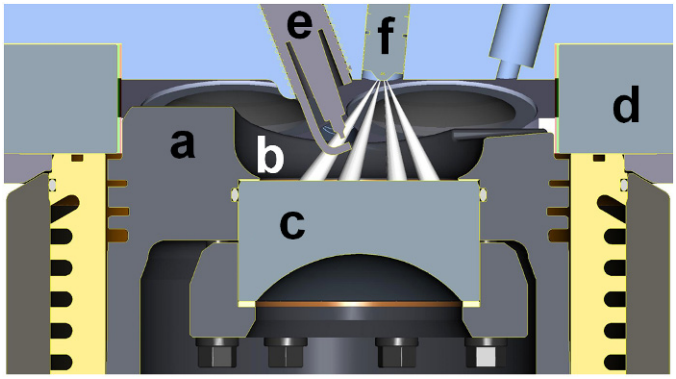

Figure 1. Cross-section of combustion chamber at TDC: a - piston, b - piston bowl, c - piston-bowl window, d - pent-roof window, e - spark plug, and f - fuel injector. Metal window blanks were used in this study.

Engine data are given in Table 1. The engine was fueled using a Bosch 8-hole step-hole Valve Covered Orifice injector. The injector was oriented such that two of the fuel sprays straddled the spark-plug gap of the commercial long-reach spark plug. For all data, the phasings of the cam shafts relative to the crank shaft were maintained constant. The cam shafts were phased to provide both low residual levels and high volumetric efficiency. A graphical representation of the valve lifts can be found in Ref. [13]. It should be noted that one intake valve was deactivated to increase in-cylinder swirl and tumble levels (see Table 1). In this study, the crank angles (CA) are referenced as after top dead center of the combustion stroke, aTDC. Exhaust-gas residual levels of this engine vary as a function of intake and exhaust pressure; in this study the residual gas level ranged from a maximum of 7% at a throttled, 60 kPa intake pressure condition, to a minimum of 3% at a lightly boosted 110 kPa intake pressure. The air was metered into the intake system using a sonic-flow nozzle.

Table 1. Engine Specifications

| | |
|---|---|
| Displacement | 0.552 liters |
| Bore | 86.0 mm |
| Stroke | 95.1 mm |
| Connecting Rod Length | 166.7 mm |
| Geometric Compression Ratio | 12:1 |
| Intake Valve Diameter | 35.1 mm |
| Intake Valve Angle Relative Cylinder Axis | 18° |
| Exhaust Valve Diameter | 30.1 mm |
| Exhaust Valve Angle Relative Cylinder Axis | 16° |
| Swirl / Tumble Index (one intake valve deactivated) | 2.7 / 0.62 |
| Fuel Injector | Bosch 8-hole solenoid-type |
| Hole Orientation | Symmetric with 60° included angle |
| Hole Size | Stepped-hole, min. dia. = 0.125 mm |

The exhaust gas flow was diluted with extra air using nozzles at the entry point of the exhaust tank. This was done to limit the exhaust gas temperature in the tank and to lower the dew point of the exhaust gases to avoid loss of unburned hydrocarbons (HC) and water due to condensation in the unheated sample lines. With precisely known exhaust dilution, the measured exhaust composition was back-corrected to engine-out mole fractions. A Horiba MEXA-584L emission analyzer measured CO, $CO_2$ and HC. $O_2$ was measured with a CAI 600PP gas analyzer. $NO_x$ was measured with a CAI 600CLD gas analyzer. Exhaust smoke was measured with an AVL 415S smoke meter.

#### Conventional Inductive Spark System

The conventional inductive system was supplied by Bosch. The spark coil (model ZS-L 1x1E) can provide relatively high spark energy. For all the tests reported here, the charging time of the primary coil was set to 5 ms. According to measurements by Bosch, this results in a spark energy of nominally 106 mJ being delivered from the secondary high-voltage coil. The secondary coil was connected to an NGK spark plug featuring a long-reach single-point J-gap. The spark gap width was adjusted to 1.0 mm prior to the engine tests.

### *Experimental Procedure and Data Analysis*

For each operating point with the all-metal engine configuration, the engine is allowed to run for several minutes until all measured parameters are stable, at which point data are acquired. Fuel-flow rate and thermocouple readouts are averaged over one minute. The in-cylinder pressure, spark current, intake and exhaust pressure, and fuel pressure are acquired for 500 consecutive cycles using 0.1°CA resolution. For the in-cylinder pressure, an uncooled Kistler 6125C piezoelectric sensor is used in combination with a Kistler 5010B charge amplifier. Day-to-day repeatability is very good, with variations of average indicated mean effective pressure (IMEP) of less than 2%.

The apparent heat-release rate (AHRR) is computed from the in-cylinder pressure for each individual cycle using a constant ratio of specific heats ($\gamma = 1.33$) following [1]. The value of $\gamma$ was chosen to yield a net-zero AHRR near the end of the compression-stroke prior to combustion. For computing combustion-phasing metrics like the 50% burn point (CA50), the AHRR is integrated over the crank-angle range for which AHRR is positive. For all data presented, this computation of burn points is performed in a conventional way, whereby the integral of AHRR is scaled so that it rises from 0 to 100% for every cycle, irrespective of the actual $\eta_{comb}$.

## *Fuels*

This study focuses on the influence of fuels composition on knock-limited operation of a directly-injected spark-ignition (DISI) engine. The three fuels used in this study were carefully designed for this purpose. The fuels were procured from Gage Products Company, who blended the fuels from refinery streams to provided specifications. Upon receipt, the fuels were sent to Southwest Research Institute (SwRI) for analysis [14], which included RON and MON testing per ASTM specifications, as well as a detailed hydrocarbon analysis (DHA), and heat of combustion measurements. Selected values from these analyses are presented in Table 2.

The three fuels used in this study have been given names for the convenience of the reader; these names are based on the composition of the fuels. For instance, the fuel named "Alkylate" is primarily composed of branched, saturated hydrocarbons (alkanes). Similarly, the "E30" fuel is comprised of 30% ethanol on a volume basis, and the "High Aromatic" fuel is comprised of a large fraction (31% by volume) of aromatic hydrocarbons.

The three tested fuels were specified to have RON ratings of 98 ± 0.5; analysis by SwRI found all three fuels met this specification within the tolerance of the RON test (0.3 ON). The RON rating was chosen as a baseline for the fuels due to its relevance to modern SI engines, while the MON ratings of the fuels were intentionally varied to provide two Octane Index [8] values for any condition not described by K = 0. The Octane Index is shown in Eq. 1, and supported by Eq. 2. From these two equations, it may be seen that OI (K=1) = MON while OI (K=0) = RON. The variation in the OI values of the fuels were achieved by specifying identical Octane Sensitivities for the two high-sensitivity fuels (High Aromatic and E30).

$$\mathbf{OI = (1 - K) \bullet RON + K \bullet MON = RON - K \bullet S} \quad \mathbf{(1)}$$

$$\mathbf{S = RON - MON} \quad \mathbf{(2)}$$

From Table 2, the E30 and High Aromatic fuels can be seen to have similar distillation curves, with nearly identical T10, T90, and TF temperatures that are within the gasoline boiling range. However, the Alkylate fuel does not exhibit a wide boiling range, as it is primarily composed of iso-octane; this is dissimilar from consumer gasolines, and reminiscent of Primary Reference Fuels, but this distillation behavior is assumed to be of minor importance for this study, due to the well-mixed early-injection strategy employed.

The fuels are assumed to have varying HoV values; this has not been measured due to the difficulty in measuring HoV for multi-component mixtures. For this study, the HoV of the Alkylate and High Aromatic fuels are assumed to be similar to commercial petroleum-based gasoline (350 kJ/kg), while the E30 is assumed to have a HoV value based on linear blending of ethanol with gasoline (533.6 J/kg). This assumption is used by GT Power to calculate the charge-cooling due to the fuel's evaporation in the combustion chamber during the intake stroke.

Table 2. Selected fuel properties and ratings for the three fuels used in this study.

| | ***Alkylate*** | ***E30*** | ***High Aromatic*** |
|---|---|---|---|
| **RON** | 98 | 98 | 98 |
| **MON** | 97 | 88 | 87 |
| **AKI (R+M)/2** | 97 | 93 | 93 |
| **Sensitivity (RON - MON)** | 1 | 10 | 11 |
| **T10 (°C)** | 93 | 61 | 59 |
| **T50 (°C)** | 100 | 74 | 108 |
| **T90 (°C)** | 106 | 155 | 158 |
| **TF (°C)** | 161 | 204 | 204 |
| **Aromatics (Vol. %)** | 0 | 8 | 31 |
| **Olefins (Vol. %)** | 0 | 5 | 4 |
| **Parafins (Vol. %)** | 100 | 57 | 65 |
| **Ethanol (Vol. %)** | 0 | 30 | 0 |
| **Net Heat of Combustion (MJ/kg)** | 44.5 | 38.2 | 43.0 |
| **Assumed Latent Heat of Vaporization (kJ/kg)** | 350.0 | 533.6 | 350.0 |
| **Average Molecular Formula** | C: 7.76<br>H: 17.45 | C: 4.49<br>H: 9.87<br>O: 0.5 | C: 6.92<br>H: 12.41 |

## *Operating Conditions*

Knock-limited CA50's (KL-CA50) were measured for each fuel over a range of operating conditions which were chosen for their relevance to modern and future engine design. These conditions are presented in Table 3. The knock-resistance of each fuel (as evaluated by KL-CA50) was tested with intake pressures ranging from 60 kPa to 110 kPa at 30 °C intake temperature, and 60 kPa to 100 kPa at 60 °C and 90 °C intake temperature (intake temperatures were measured in the intake runner). These intake conditions yielded a range of KL-CA50's from overly advanced at 60 kPa (combustion phasing advanced from MBT timing: 8 – 10 CAD aTDC) to highly retarded at 110 kPa (combustion phasing approaching 30 CAD aTDC). These conditions could be encountered by a future high-efficiency, high compression ratio, naturally-aspirated DISI engine when using a highly knock-resistant fuel similar to those used in this study. Also of

interest are conditions that may be encountered by future high-efficiency boosted DISI engines; however, this is beyond the scope of the present study, though plans are in place to investigate these conditions (see Future Work section at the end of this manuscript).

Table 3. Operating conditions for fuel, intake pressure, and intake temperature sweeps of KL-CA50.

| Variable | Range |
|---|---|
| Fuel | Alkylate, High Aromatic, E30 |
| Intake Temperature | 30, 60, 90 °C |
| Intake Pressure | 60, 80, 100, 110 (30 °C only) kPa |

## *Knock Intensity Calculation*

To quantify the acoustic noise generated by rapid autoignition-based combustion of the end-gas, an in-house developed metric named Knock Intensity (KI) was used. It is based on the measured in-cylinder pressure, which is processed on a cycle-by-cycle basis over several steps.

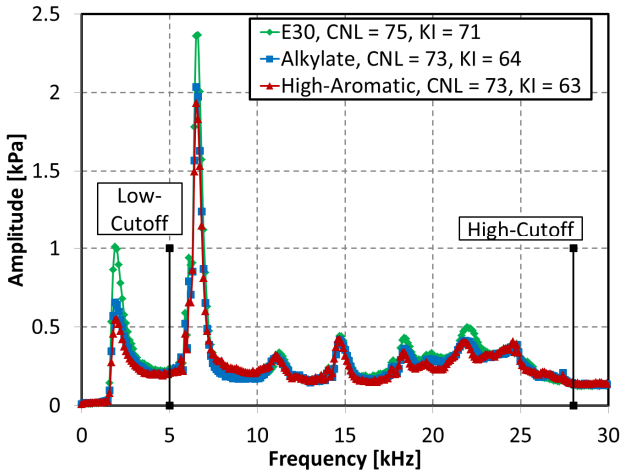


Figure 2. Frequency content of three measured pressure traces under "light" knocking conditions, yielding KI values that correspond to Knock-Limited combustion phasing. Also shown are the low- and high-frequency cutoffs in relation to the frequency range which contributes to the KI value (5 – 28 kHz).

The measured pressure trace was first low-pass filtered (<1.5 kHz). This low-pass filtered pressure trace was then subtracted from the unfiltered trace, effectively rendering a high-pass filtered pressure trace. Lastly, using Fourier decomposition, the energy content in the 0 – 80 CAD aTDC range was summed over the frequency range of 5 – 28 kHz. The crank-angle range was limited to increase signal-to-noise of this KI metric. The specific frequency range was chosen to capture the pressure oscillations related to knocking combustion, but to avoid those oscillations related to noise in the sensor or data acquisition system (> 28 kHz) or to the piston motion and deflagration-based combustion (< 5 kHz). The reported KI values correspond to the average over 500 cycles. Figure 2 provides examples of the frequency content of lightly-knocking pressure traces for the three tested fuels. Also included are their respective computed KI's and Combustion Noise Levels (CNL's) [15]. This figure illustrates the chief oscillatory frequencies due to knock and normal combustion. It may be seen that these three fuels exhibit similar frequency content, allowing the use of a fixed frequency range for this analysis.

## *Knock-Limited CA50 Measurement Procedure*

A key metric of this study are the Knock-Limited Combustion Phasings (KL-CA50's) of each fuel over a range of operating conditions. Each KL-CA50 was measured by fixing intake pressure and temperature, and varying spark timing until the steady-state average combustion phasing resulted in a KI between 60 and 80, with a value of 70 being the target. At this KI level, the engine operation exhibited knock that was audible above the mechanical noise of the engine for a large fraction of the cycles. In addition, a large fraction of the cycles display a second AHRR peak, corresponding to the enhanced combustion rate due to end-gas autoignition. As such, the engine operation was harsher than what is tolerable for automotive engine calibration, but such operation with clearly distinguished knock facilitated this parametric knock study.

Figure 3 shows that the KI values obtained were highly dependent on CA50 under the investigated conditions. To this end, spark timing was controlled in 0.1 CAD increments, which enabled CA50 control on a similar scale. Figure 3 also shows that KI varied significantly over a range of 1 CAD, indicating that small variations in KI among the measured operating points did not significantly affect the determination of KL-CA50. Even so, it should be noted that knock statistics vary both with fuel type and operating conditions, as discussed the last result section preceding the Conclusions.

The repeatability of the measurement was checked by comparison of data points obtained during a preliminary exploration with those taken approximately 3 months later during the main period of data collection. Of the overlapping (comparable) operating conditions, KL-CA50 varied on average by 0.6 CAD, while the largest variation was 1.2 CAD (at a highly-retarded combustion phasing operating point). Therefore, in this study, variations in KL-CA50 among the fuels is only considered significant when the variation exceeds 1 CAD.

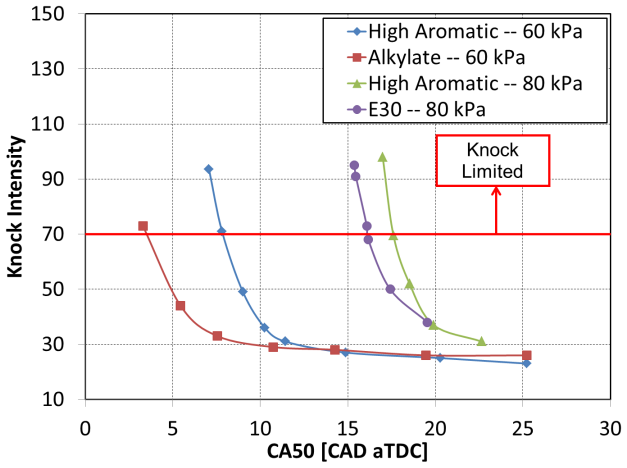


Figure 3. Variation of Knock Intensity with average combustion phasing (CA50). Presented here are combinations of fuels and operating points; all conditions use a 30 °C intake temperature. The Knock Intensity threshold of 70 is indicated. Spark timing was varied in 0.1 CAD increments, though only operating points which were allowed to converge to steady state are plotted.

### *Calculation of Unburned Zone Temperature*

The mass-averaged temperature of the unburned charge throughout the closed cycle was calculated using the commercial software GT Power [16]. The model included both intake and exhaust systems and a significant amount of time was spent calibrating the model to reproduce motored cylinder pressure traces and system mass flow rates across a wide range of conditions that far exceed those encountered in this study. In addition, the direct-injection evaporation process was calibrated to reproduce mass-flows and cylinder pressure for unfired fuel-injection cases.

Measured pressure traces were input to GT Power and used to calculate the heat release rate, burned fraction, and in-cylinder temperature using a two-zone (burned- and unburned-zone) model. In the model, under conditions in which pre-flame heat release was observed experimentally, the spark timing was set to the point at which deflagration based heat release was first measurable. This approach prevented the formation of a burned zone within the model until deflagration based combustion began in earnest.

As knock is a stochastic event, individual pressure cycles were used for calculations rather than an average pressure trace. In order to have an end-gas autoignition that was clearly distinguishable from the deflagration based combustion, the highest KI cycles were used for this analysis, and a representative cycle (of heavy knock) was chosen from this ensemble for use in figures. In the figures which include temperature-pressure histories, the end of the trace represents the point of auto-ignition, which was determined from the minimum point of the AHRR trace between the deflagration and auto-ignition heat release.

## Results

### *Effect of Intake Pressure on Knock-Limited CA50*

KL-CA50 was measured for three fuels under stoichiometric, undiluted operation with intake temperatures of 30 °C, 60 °C, and 90 °C at 60 kPa, 80 kPa, 100 kPa, and 110 kPa (30 °C only) intake pressures in the manner described in the preceding section and as shown in Table 3. The results of the 30 °C experiments are presented in Figure 4, which also indicates an approximate combustion phasing retard beyond which cycle efficiency is impacted. Figure 4 illustrates the similarities and differences of the fuels' auto-ignition behavior, and their response to intake pressure, may be seen. Figure 4 indicates that while all three fuels display similar knock resistance at conditions near naturally aspirated (80 – 110 kPa), the fuels exhibit dissimilar behavior with regards to varying intake pressure. Of the three fuels, the E30 blend yielded the most linear trend between intake pressure and KL-CA50, while the other high-sensitivity fuel, the High-Aromatic blend, also exhibiting relatively linear variation of KL-CA50 with intake pressure, with some deviation at the highest intake pressure tested (110 kPa). Conversely, the Alkylate fuel's KL-CA50 varies in a non-linear manner with intake pressure; this fuel shows a clear advantage in knock-resistance at low intake pressure (60 kPa), while at higher intake pressures the Alkylate fuel behaves similarly to the other two fuels.

Considering the RON and MON ratings of the three fuels (all three fuels share the same RON rating, while the Alkylate holds a higher MON rating) and the KL-CA50 measurements, it may be surmised that the higher intake pressure conditions correlate more closely with the RON ratings, as indicated by the similar performance of the fuels at this condition, while the 60 kPa condition moves in the direction of the MON condition, as evidenced by the superior performance of the Alkylate fuel at this condition. This behavior agrees with the behavior previously demonstrated by [17] and [18], namely that higher pressures for a given temperature correspond to lower Octane Index K values (see Eq. 1 and 2).

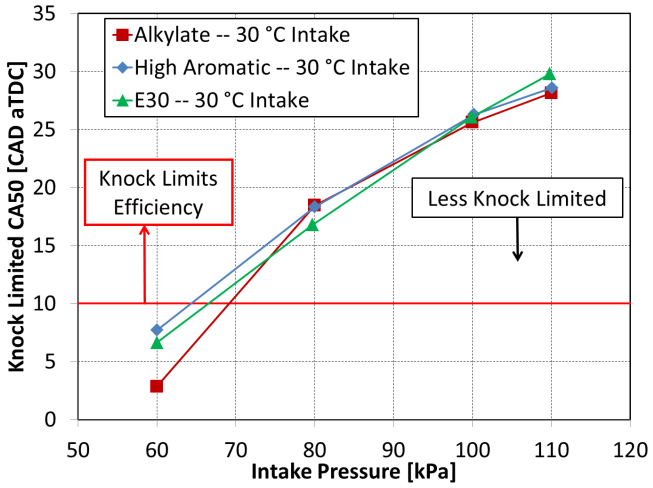


Figure 4. KL-CA50 behavior of the three tested fuels at 30 °C intake temperature, stoichiometric, un-diluted conditions, and KI limit = 70.

The variation of KL-CA50 with intake pressure was found to be influenced by the low-temperature chemistry of the fuels, as evaluated by the magnitude of low-temperature heat release (LTHR) observed in the calculated AHRR traces for each operating condition. Figure 5 a) shows the cylinder pressure profiles for the three tested fuels at the KL-CA50 condition with 110 kPa intake pressure and 30 °C intake temperature, while Figure 5 b) shows the AHRR's which have been calculated from the pressure traces in Figure 5 a). It may be seen in the zoomed-in version of Figure 5 b), Figure 6, that the fuels displayed significantly different magnitudes of LTHR at this 110 kPa intake pressure condition, which can be seen here as the heat release bump that occurred prior to the main deflagration-based combustion (and primarily ahead of the spark timing which is marked on the figure). At this operating point, the Alkylate fuel exhibited the highest magnitude (both peak and integrated) of LTHR, while the Aromatic fuel exhibited significantly less LTHR, and the E30 exhibited the least LTHR. LTHR has been shown to be highly dependent on operating conditions [19, 20], and this behavior was observed in the current work. Specifically, the fuels exhibited higher levels of LTHR as intake pressure was increased, as seen in Figure 7, which presents AHRR profiles for the Alkylate fuel at 60, 80, 100, and 110 kPa intake pressures. Figure 7 demonstrates that as intake pressure was increased, the Alkylate fuel exhibited great magnitudes of LTHR. The magnitude of LTHR has previously been found to be sensitive to the concentration of molecular oxygen [21], which limits the rate of low-temperature chain-branching of saturated hydrocarbons. In an engine environment, LTHR typically varies with intake pressure and EGR levels [19], as this varies the concentration of oxygen at the temperatures which are relevant for the low-temperature chain branching pathway (500 – 800 K).

The intake pressure dependence described in the preceding paragraph was observed for all three tested fuels. However, the critical intake

pressure at which each fuel began to exhibit LTHR varied across the fuels. The Alkylate fuel was found to have the greatest tendency towards LTHR, and at the 30 °C intake temperature condition, it exhibited measurable LTHR at intake pressures of 80 kPa and above. In contrast, the two high Octane-Sensitivity fuels, the E30 blend and the Aromatic blend, exhibited less tendency towards LTHR, requiring higher intake pressures to yield measurable LTHR. In the case of the Aromatic fuel, 100 kPa intake pressure was required for LTHR, while the E30 fuel required 110 kPa to exhibit LTHR.

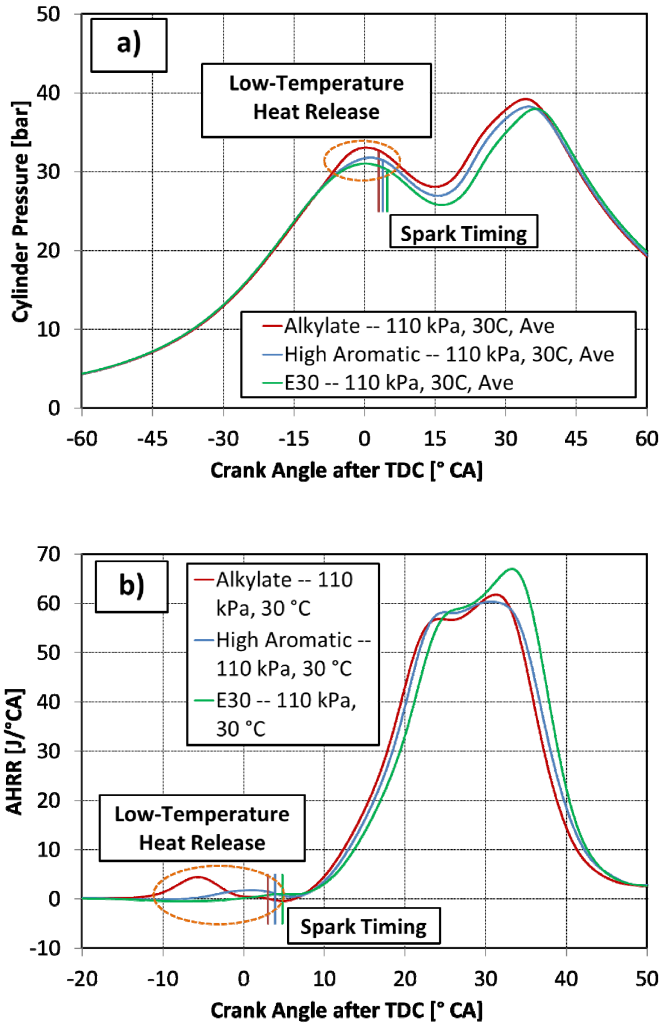


Figure 5. Ensemble-average a) pressure traces and b) calculated Apparent Heat Release Rate traces of the three tested fuels at KL-CA50 conditions with 110 kPa intake pressure and 30 °C intake temperature. KL-spark timing is indicated using vertical lines in both a) and b).

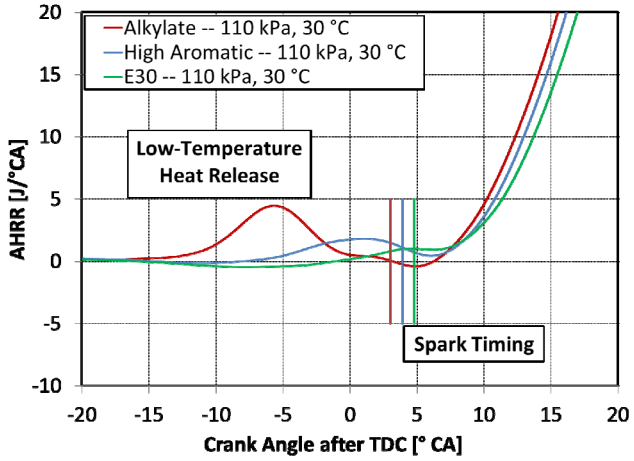


Figure 6. Zoomed-in reproduction of Figure 6 b) to allow examination of the pre-spark heat release. KL-spark timing is indicated with vertical lines.

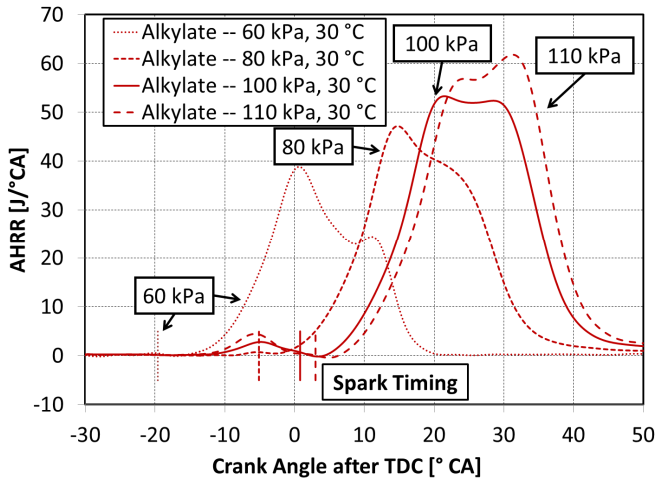


Figure 7. Ensemble averaged AHRR behavior of the Alkylate fuel at 30 °C intake temperature with KL-CA50 as intake pressure varied from 60 to 110 kPa. KL-spark timing is indicated with vertical lines.

## *Unburned-Charge Temperature and Pressure Histories*

Low-temperature chain branching and heat release typically enhance the auto-ignition process through combined thermal and chemical effects; this has been witnessed in both fundamental combustion experiments [22, 23] and homogeneous charge compression ignition engine experiments [20, 21]. The thermal effect of the heat release is an increase in charge temperature over that of a non-reacting situation. The chemical effect of low-temperature chain branching is the formation of radical and reactive intermediate species that enhance the hot-ignition process. For this reason, it is posited that the observed LTHR may influence the measured knock-limits of the SI combustion system, as engine knock is fundamentally caused by an auto-ignition process of the end-gas. The temperature and pressure histories of the end gas leading up to autoignition were calculated in an effort to help assess the many factors contributing to autoignition of the tested fuels. Temperature and pressure histories for heavy-knocking individual cycles are plotted in Figure 8, for the three tested fuels, at both 60 and 110 kPa intake pressures, and 30 °C intake temperature. These graphs indicate the trajectories of the end-gas under different operating conditions. It may be seen in Figure 8 that

while all three fuels are rated with the same RON, and two of the three fuels with the same MON, they experienced significantly different conditions leading up to auto-ignition, with some of these differences stemming from slightly different KL-CA50's between the fuels, and other differences stemming from the fuels' differing composition. Specifically, the temperature and pressure histories of the fuels were influenced by the fuel's heat of vaporization, the specific heat ratio of the fuel-air mixture, the spark-ignition timing and subsequent heating of the end-gas, and the amount of heat release by the fuel prior to auto-ignition, typically in the form of LTHR.

Examining Figure 8, significant differences among the three fuels may be seen, at both the 60 and 110 kPa intake pressure conditions. First, at both intake pressures, the E30 charge begins the closed cycle at a lower temperature than the Aromatic or Alkylate fuels, due to the higher HoV and the amount of E30 required to form a stoichiometric mixture with air than traditional gasoline and air. The lower charge temperature of the E30 continues throughout the cycle, and E30 auto-ignites at the lowest temperatures and pressures of the tested fuels. Next, at 110 kPa intake pressure, the Alkylate and High Aromatic fuels yield similar charge temperatures throughout the early portion of the compression stroke, but then begin to diverge near TDC. This divergence was due to LTHR, resulting in a higher temperature for the Alkylate fuel than the High Aromatic fuel near and after TDC. This difference continues to the point of auto-ignition, which consistently occurs at the highest temperatures for the Alkylate fuel, at a given set of intake conditions. Finally, differences in spark timing alter the deflagration-based combustion, which in turn alters the amount of compression that the end-gas undergoes due to flame propagation. However, by nature of the similar KL-CA50's of the three fuels, differences in the deflagration process were not large; CA10 to CA90 burn durations varied less than 1 CAD for the 110 kPa condition across the three fuels.

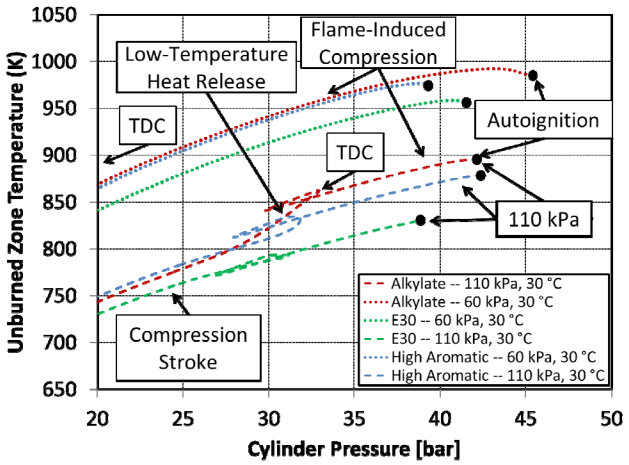


Figure 8. Temperature and pressure histories of the end-gas of the reacting charge leading up to the point of autoignition for the three tested fuels at 60 and 110 kPa intake pressures. Plotted traces are computed by GT Power as described in the Calculation of Unburned Zone Temperature section of this manuscript. Traces are computed from an individual cycle representative of strong end-gas auto-ignition. Pressure traces vs. crank-angle and AHRR vs. crank angle for 110 kPa are shown in Figure 5 a) and b).

To recap the observations at 110 kPa, Figure 8 indicates that the E30 fuel is the least resistant to high temperatures and pressures, but by nature of its high charge cooling and low tendency to exhibit low-temperature chain branching, it offers similar practical knock resistance to the other two fuels. The Aromatic fuel auto-ignites at temperatures between the E30 and Alkylate fuels, and by having less charge cooling than the E30, but less LTHR than the Alkylate, the end result is similar engine performance to the other two fuels under the tested conditions. Finally, the Alkylate fuel has the greatest resistance to autoignition in terms of end-gas temperature and pressure, but by nature of having the greatest magnitude of LTHR, the practical knock resistance of this fuel is similar to the High Aromatic and E30 fuels.

However, revisiting Figure 4, while the three fuels have similar KL-CA50 at higher intake pressure conditions, their knock resistance measurably diverges at lower intake pressure conditions. At lower intake pressures, none of the fuels exhibited LTHR. Thus, the primary variations in temperature and pressure histories are due to differences in HoV charge cooling of the fuel-air mixtures and the effects of spark phasing on flame-induced compression, which when combined result in lower end-gas temperatures for the E30 fuel than the other two fuels. Similar to the behavior exhibited at the 110 kPa intake pressure condition, the Alkylate fuel exhibits the greatest autoignition resistance to end-gas temperature and pressure. However, with no heating of the end-gas due to LTHR at the 60 kPa condition, this meant that the Alkylate fuel allowed significantly more advanced combustion phasing over the other two fuels, while the E30's additional charge cooling provided a slight advantage over the Aromatic fuel.

The behaviors described above are still consistent with the RON and MON ratings of the fuels. At higher intake pressures and retarded combustion phasings, the fuels exhibited similar KL-CA50 behavior, which is consistent with their identical RON ratings. At lower intake pressures, as combustion phasing was advanced, the Alkylate fuel began to show a clear advantage over the other two fuels, which indicates a shift towards MON conditions. These observations are in line with knowledge of the conditions probed by the RON and MON tests, with the RON test emphasizing lower-temperature auto-ignition resistance, and the MON test emphasizing higher-temperature auto-ignition resistance [24].

### *Effects of Intake Temperature on Knock-Limited CA50*

In addition to measuring the sensitivity of KL-CA50 to intake pressure for each fuel, sensitivity of KL-CA50 to intake temperature was also assessed, by measuring KL-CA50 at 60 °C and 90 °C intake temperatures in addition to the 30 °C results which were previously presented and discussed.

Figures 9, 10, and 11 plot the KL-CA50 of each fuel at the three measured intake temperatures (30, 60, 90 °C) and three intake pressures (60, 80, 100 kPa). The information contained in Figure 9 – 11 is distilled into a single plot in Figure 12. The KL-CA50 of the fuels varied as conditions deviated from the 100 kPa intake pressure, 30 °C intake temperature operating condition. The two high octane-sensitivity fuels behaved similarly, while the Alkylate fuel exhibited greater knock resistance under lower intake pressure and higher intake temperature conditions. In addition, the KL-CA50 responses to increased intake temperature differed among the three fuels, and further varied non-monotonically with intake pressure. Specifically, Figure 9 shows that in the case of the Alkylate fuel, two disparate responses to intake temperature are observed. At 60 kPa intake pressure, increased intake temperature retarded KL-CA50 by enhancing the potential for end-gas auto-ignition. However, at 80 and 100 kPa intake pressures, increased intake temperatures allowed an advance of KL-CA50. This result may seem surprising as Arrhenius-type reaction rates, which govern the auto-ignition process, increase

with temperature such that ignition delay times typically decrease with temperature. However, the increased temperature reduced the magnitude of LTHR, removing the thermal and chemical reactivity benefit provided by LTHR, such that the end-gas was overall less reactive. Decreased reactivity with increased temperature is often referred to as Negative Temperature Coefficient (NTC) behavior. Exploitation of the NTC behavior of gasoline fuels in SI engines may allow operation strategies that use earlier combustion phasing under operating conditions for which this behavior exists.

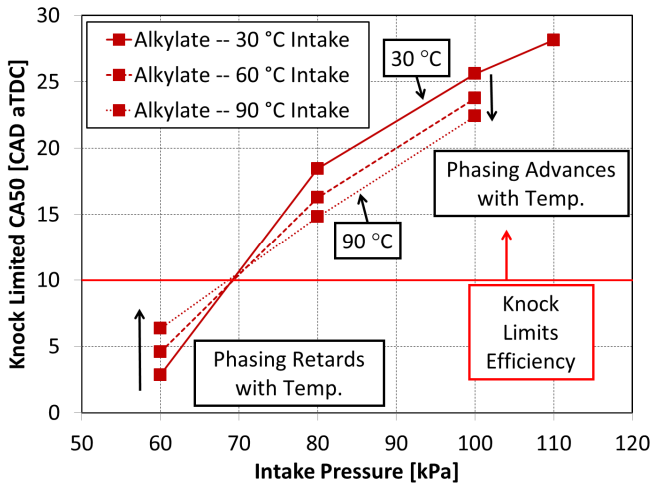


Figure 9. KL-CA50 behavior of Alkylate fuel over the range of tested intake pressure (60 – 110 kPa) and intake temperature (30 – 90 °C) conditions.

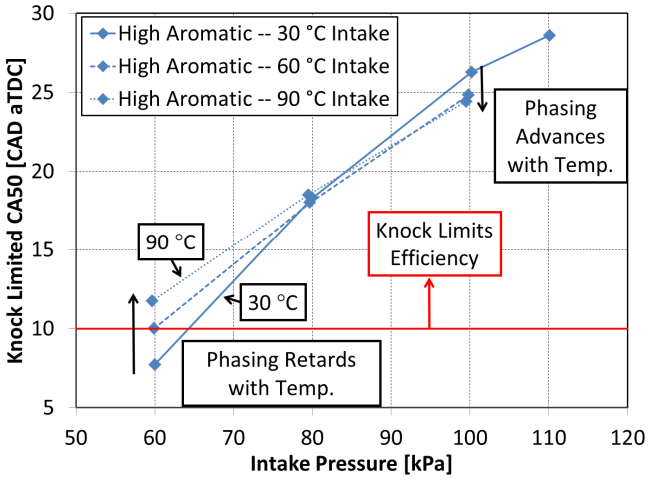


Figure 10. KL-CA50 behavior of High Aromatic fuel over the range of tested intake pressure (60 – 110 kPa) and intake temperature (30 – 90 °C) conditions.

NTC behavior in hydrocarbon fuels is typically caused by a shift in the dominant chemical pathway from the low-temperature chain-branching pathway (T < 850 K) to the intermediate-temperature regime (850 K < T < 1000 K) in which chain propagation and termination, rather than branching, dominate the kinetic process [21]. Due to the pressure sensitive rate of O2 addition at the start of the low-temperature chain branching pathway, LTHR has been observed in [23, 25] to be highly sensitive to [O2]. This understanding of low-temperature chain branching kinetics suggests that the LTHR was suppressed in the heated intake temperature experiments due to the different temperature-pressure trajectory followed by the charge.

Specifically, given the fixed compression ratio and intake pressure, the heated intake temperature experiments yielded a higher charge temperature for a given pressure (as will be discussed in detail later in this section). Because the heated intake temperature experiments traversed the low-temperature pathway temperature-range (T < 850 K) at a lower in-cylinder pressure and [O2], the overall rate of the pathway, and consequently the LTHR magnitude, was reduced.

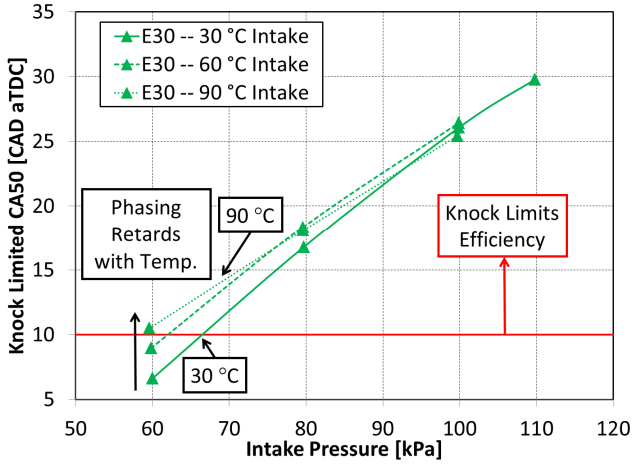


Figure 11. KL-CA50 behavior of E30 fuel over the range of tested intake pressure (60 – 100 kPa) and intake temperature (30 – 90 °C) conditions.

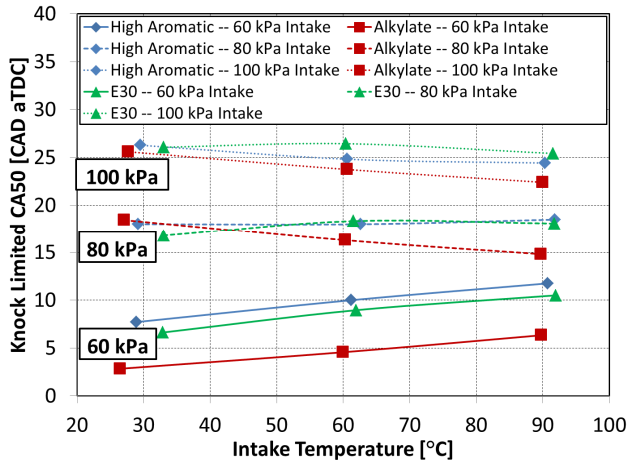


Figure 12. Variation of KL-CA50 with intake temperature for the three tested fuels at 60, 80, and 100 kPa intake pressure.

The reduction in the magnitude of LTHR that occurred prior to combustion for increased intake temperature was a key factor in determining the different trends that were observed at different intake pressure conditions. In the case of the Alkylate fuel at 60 kPa intake pressure, no LTHR occurs at the lowest intake temperature (30 °C), and thus as intake temperature is increased, the end-gas temperature increases significantly. However, at 100 kPa intake pressure and 30 °C intake temperature, the Alkylate fuel exhibited a significant magnitude of LTHR, and as intake temperature was increased, the LTHR decreased. This behavior is shown in Figures 13, 14, and 15. In Figure 13, AHRR's are plotted for the Alkylate fuel at 100 kPa intake pressure and 30, 60, and 90 °C intake temperature. Figure 14 shows this same information, but with magnification of the pre-spark region. Figure 15 plots the temperature and pressure histories of the

three cases shown in Figures 13 and 14. From Figure 15, it may be seen that as intake temperature was increased and LTHR magnitude decreased, there was a corresponding effect on the end-gas temperature and pressure. Specifically, the result of the higher IVC temperature may be seen in the differences between the fuels in the left-half of the figure, prior to LTHR, TDC, and spark-timing. However, Figure 15 shows that by nature of the varying LTHR magnitude and spark timings, nearly identical end-gas autoignition temperatures were achieved. Finally, as evidenced by the measured KL-CA50, the decrease in LTHR magnitude must have had a combined thermal and chemical effect on the end gas that outweighed the intake temperature increase.

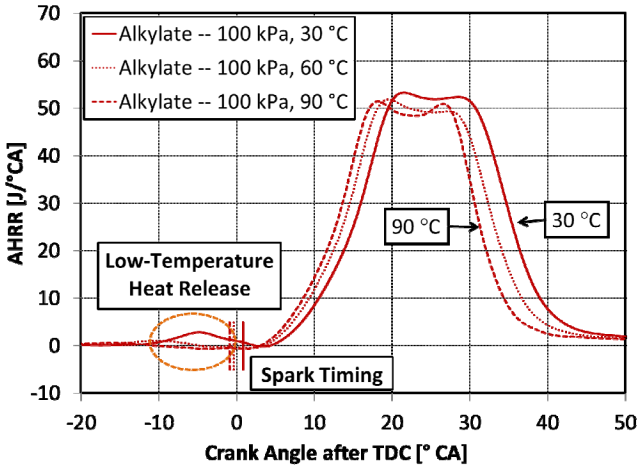


Figure 13. Ensemble-average Apparent Heat Release Rate traces of the Alkylate fuel at KL-CA50 conditions with 100 kPa intake pressure and 30 °C, 60 °C, and 90 °C intake temperature.

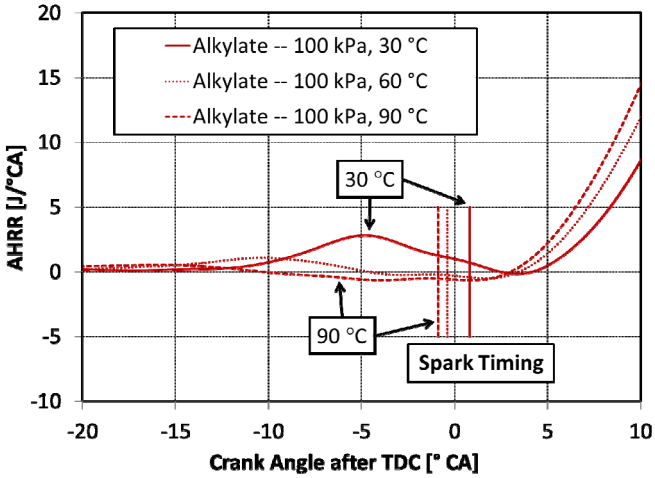


Figure 14. Zoomed-in reproduction of Figure 10 to allow examination of the pre-spark heat release.

Returning to the case of the 60 kPa intake pressure, Figure 16 plots the end-gas pressure and temperature histories leading to autoignition for both 30 and 90 °C intake temperature cases. The two histories plotted in Figure 16 indicate that similar temperatures were reached prior to autoignition, though by nature of the retarded spark timing at the 90 °C intake temperature condition, the end-gas for this case does not reach as high a pressure as the 30 °C case. Similar temperatures in the 900 – 1100 K range at the point of auto-ignition are indicative of fuel auto-ignition via the high-temperature pathway, which is driven by fuel decomposition by β-scission [22].

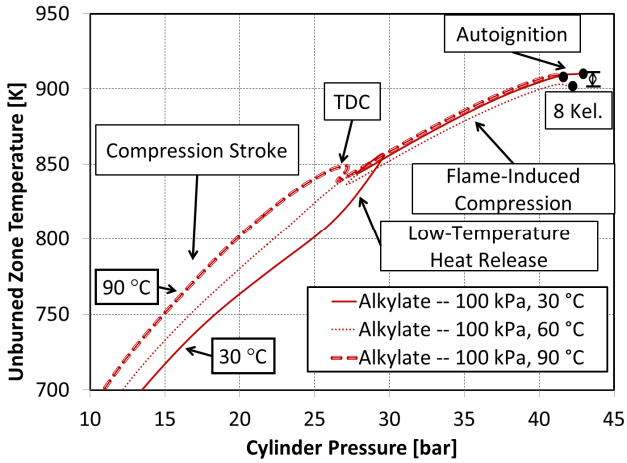


Figure 15. Temperature and pressure histories of the end-gas of the reacting charge leading up to the point of autoignition for the Alkylate fuel at 100 kPa intake pressure and 30 °C, 60 °C, and 90 °C intake temperature. Plotted traces are computed by GT Power as described in the Calculation of Unburned Zone Temperature section of this manuscript. Traces are computed from an individual cycle representative of strong end-gas auto-ignition.

The Alkylate fuel has served as an example of the response to increased intake temperature, but the underlying behavior was similar for all three fuels. However, this is not to say that the Aromatic and E30 fuels behaved identically to the Alkylate fuel, because the three fuels began to exhibit LTHR at varying intake pressures. This, in turn, varied the responses of the fuels to intake temperature, when intake pressure was held constant.

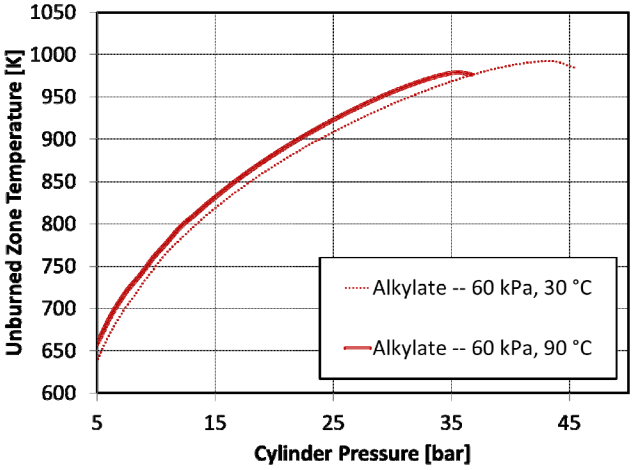


Figure 16. Temperature and pressure histories of the end-gas of the reacting charge leading up to the point of autoignition for the Alkylate fuel at 60 kPa intake pressure and 30 °C and 90 °C intake temperature. Plotted traces are computed by GT Power as described in the Calculation of Unburned Zone Temperature section of this manuscript. Traces are computed from an individual cycle representative of strong end-gas auto-ignition.

Figure 12 replots the data from Figures 9 – 11, but now against intake temperature. Due to the absence of LTHR at 60 kPa intake pressure, both the Aromatic and E30 fuels required phasing retard with increased intake temperature, and this retard was of a similar magnitude to the Alkylate fuel at this intake pressure. This can also be seen in Figures 17, which plots the slope of the KL-CA50 the slope of the KL-CA50 response to intake temperature, for each intake pressure. Figure 17 shows that the Aromatic and E30 fuels had a similar response to temperature, while the Alkylate fuel deviated strongly for the intermediate intake pressure. The Alkylate fuel transitioned from phasing advance to retard as intake pressure was increased from 60 to 80 kPa, the Aromatic and E30 fuels transitioned from phasing advance to retard more gradually, over the range of 60 to 100 kPa. The more gradual transition for the Aromatic and E30 fuels corresponded with a more gradual onset of LTHR with pressure. The E30 fuel, which had the lowest magnitudes of LTHR, benefited the least from increased intake temperatures, generally displaying retarded combustion phasing as temperature was increased.

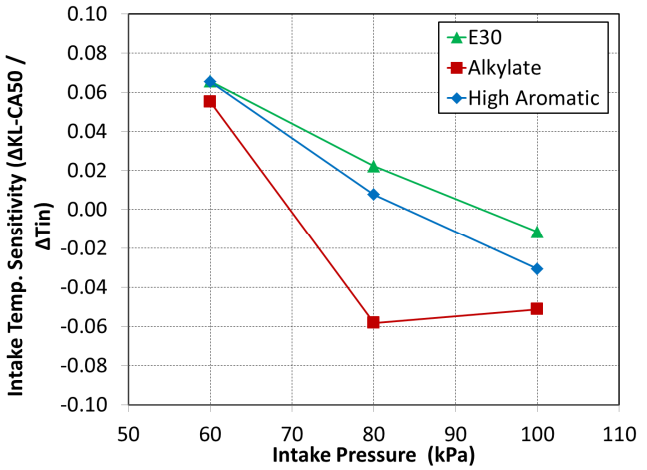


Figure 17. Sensitivity of KL-CA50 to intake temperature for the three tested fuels at three intake pressure conditions: 60, 80, and 100 kPa. Positive values indicate phasing retard with increased temperature, negative values indicate phasing advance with increased temperature.

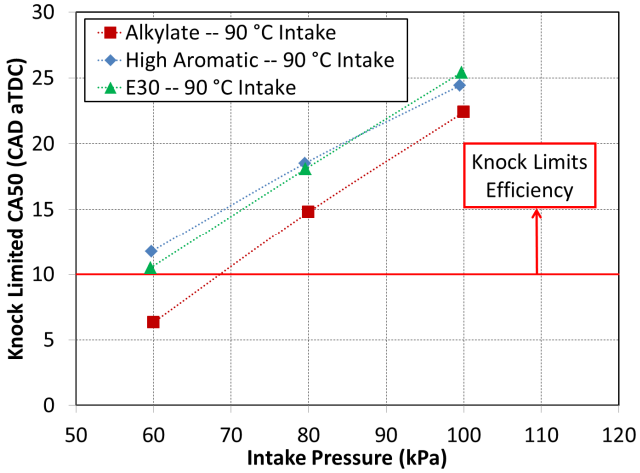


Figure 18. KL-CA50 behavior of the three tested fuels at 90 °C intake temperature, stoichiometric, un-diluted conditions, and KI limit = 70.

Having considered and assessed the various changes to temperature and pressure trajectories that occurred as intake temperature was raised, it is now appropriate to assess the sum of these factors on the knock resistance of the fuels, as seen in the 90 °C intake temperature KL-CA50 measurements presented in Figure 18 (this figure includes data previously presented in Figures 9, 10, and 11, for the sake of cross-fuel comparisons). From this figure it may be seen that, at the 90 °C intake temperature condition, the Alkylate fuel allowed for more advanced KL-CA50 operation than the High Aromatic and E30 fuels, now not only at 60 kPa intake pressure but also at 80 and 100 kPa intake pressures. As previously discussed, this was due to the suppression of the low-temperature heat release in the Alkylate fuel, which reduced the end-gas temperature later in the cycle, allowing the spark timing to be advanced to compensate. It may also be noted from examination of Figure 18 that the High Aromatic and E30 fuels behave similarly to one another. These results indicate that the RON and MON ratings of the fuels are sufficient to describe their knock-limited behavior at these conditions (when applying appropriate Octane Index K values, in this case K > 0). Two dissimilar fuels with matching RON and matching MON ratings (and thus Octane Index rating) behave identically (considering the precision of the measurement described in the Knock-Limited CA50 Measurement Procedure section) while the fuel with an identical RON and a different MON rating performs better than the other two fuels. This result indicates the strength of RON and MON ratings over a range of conditions, as well as the importance of high MON ratings under certain operating conditions.

## *Cycle-to-Cycle Variations: Characteristics and Effects on Knocking Intensity*

In addition to the measurement and analysis of KL-CA50 for a variety of conditions, an analysis of the statistical distributions of knocking behavior was performed. SI engine knock is known to be a stochastic event. The stochasticity is caused by in-cylinder turbulence, which influences a number of factors related to local conditions in the cylinder, but most importantly, the velocity and turbulence level in and around the spark-plug gap during the spark event. This local velocity and turbulence level affects the early flame development time, causing cycle-to-cycle variations in flame propagation and combustion phasing.

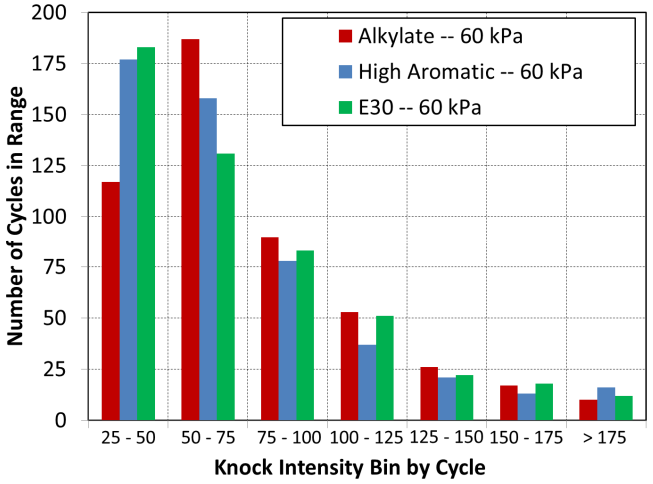


Figure 19. Knock Intensity of individual cycles (500 total) for an ensemble average Knock Intensity ~ 70 with 60 kPa intake pressure and 30 °C intake temperature for the three tested fuels.

Figure 19 plots the number of cycles, out of 500 total, which fall into various bins of KI, for a 60 kPa intake pressure and 30 °C intake temperature condition. It can be seen from Figure 19 that under this condition, the fuels exhibit similar distributions of knock intensity. However, as intake pressure was increased to 100 kPa, as shown in Figure 20, the fuels exhibit significantly different distributions of KI over the measured cycles. Figure 20 shows that at the 100 kPa condition, the Alkylate and High Aromatic fuels both yielded approximately 300 out of 500 cycles each in the lowest KI bin, 0 – 50 KI, which corresponds to a non-knocking condition. Conversely, the E30 fuel produced only approximately 200 out of 500 cycles in this KI range.

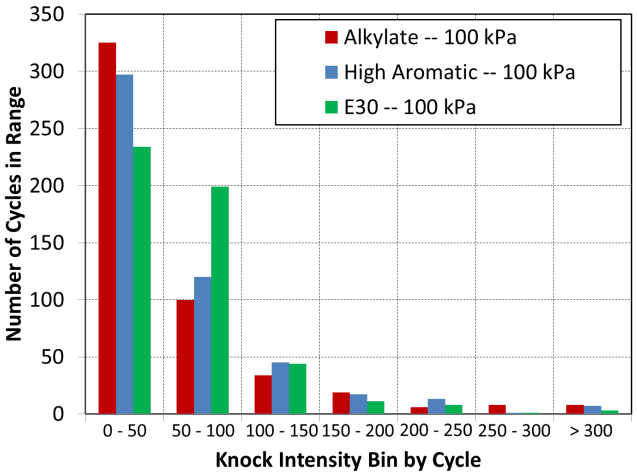


Figure 20. Knock Intensity of individual cycles (500 total) for an ensemble average Knock Intensity ~ 70 with 100 kPa intake pressure and 30 °C intake temperature for the three tested fuels.

The differences in distributions among the fuels are carried throughout the range of measured KI's. The E30 fuel yielded a large number cycles that could be described as "lightly" knocking – KI = 50 – 150 – and a lower number of "heavy" knocking cycles – KI > 300 – when compared to the other two fuels. This is borne out in Table 4, which presents statistics on the 100 kPa condition. Of the three fuels, the E30 has the highest average knock intensity, but the lowest number of cycles with KI > 200. Interestingly, the fuels have similar levels of cycle-to-cycle variation in CA30, which may be taken as a marker of variations due to early flame development, as well as similar variation of CA50 and CA70. Therefore, it is posited that differences in the fuel auto-ignition chemistry yield different distribution of knocking cycles even when the combustion phasing variability is quite similar. Finally, this phenomenon was extremely repeatable, with data points acquired at the beginning and the end of the study yielding nearly indistinguishable distributions. However, the mechanism for this behavior remains under investigation. Nonetheless, these differences in KI distribution can be important due to their implications on knock mitigation for production vehicles. For example, if the engine calibration is targeting stringent NVH standards, the E30 fuel may be more favorable than indicated by the KL-CA50 trends in Fig. 4.

Table 4. Average and statistical variation of knock intensity at Knock-Limited Combustion Phasing with 100 kPa intake pressure and 30 °C intake temperature.

| 100 kPa Intake Pressure | | | |
|---|---|---|---|
| Fuel | Alkylate | High Aromatic | E30 |
| Average Knock Intensity | 64 | 67 | 67 |
| Standard Deviation of Knock Intensity | 65 | 66 | 46 |
| Standard Deviation of CA30 (CAD) | 1.24 | 1.17 | 1.22 |
| Standard Deviation of CA50 (CAD) | 1.42 | 1.36 | 1.39 |
| Standard Deviation of CA70 (CAD) | 1.52 | 1.47 | 1.53 |
| Percentage of Cycles KI > 200 | 4.4% | 4.2% | 2.4% |

## Conclusions

This study investigates the hypothesis that fuel properties can describe the performance of a fuel in a DISI engine, evaluated here as the resistance to end-gas autoignition. To this end, three custom blended fuels which controlled RON and MON but varied in molecular composition were tested for knock-limited combustion phasing (KL-CA50) over a range of intake pressure and temperature conditions in a modern prototype, high-swirl (by nature of intake valve deactivation), DISI engine. The three fuels, which shared a RON = 98, were found to have similar KL-CA50 performance at 80 and 100 kPa intake pressure conditions. However, the performance of the fuels diverged slightly under 60 and 110 kPa intake pressure conditions. This divergence was due to the different manners in which each fuel resists knocking; the three fuels exhibited different tolerances to end-gas temperature, different levels of end-gas heating from LTHR, and different levels of evaporation cooling due to each fuel's HoV. These factors combined at 80 and 100 kPa intake conditions to yield very similar knock resistance, as indicated by the fuels' shared RON values. However, as operating conditions were changed, by varying either intake temperature or pressure, the factors yielding knock-resistance for the three fuels fell out of balance. Specifically, at low intake pressures and high intake temperatures, LTHR magnitude was reduced. Decreasing LTHR magnitude reduced the end-gas temperature and pressure; the largest effect was to the Alkylate fuel, which had the strongest tendency to exhibit LTHR, and therefore under low-pressure and high-temperature conditions, this fuel performed the best as LTHR was reduced. The observed behavior was in good agreement with prior knowledge of the RON and MON ratings; at conditions which more resembled the MON test, the Alkylate performed the best, while under RON-like conditions, all three fuels behaved similarly. In addition, the HoV benefit provided by ethanol addition was observed in the end-gas temperature and pressure histories which were analyzed; however, the E30 fuel's lower resistance to end-gas temperature and pressure balanced this effect.

To summarize:

1. The three tested 98 RON fuels exhibited indistinguishable knock-limited combustion phasings at naturally aspirated conditions. This indicates that the RON test is sufficient to

describe the autoignition resistance of the fuels under this condition, indicating an Octane Index K = 0 condition.

2. The three tested fuels exhibited measurably different knock-limited combustion phasings at a low intake pressure condition (60 kPa) as well as at high intake temperature conditions (90 °C). However, at conditions under which the KL-CA50 behavior diverged, it did so in a manner consistent with the RON and MON ratings, when considering them in the framework of the Octane Index.

3. Each fuel had a different response to intake pressure, resulting in distinguishable KL-CA50's at intake pressure conditions other than 80 – 100 kPa.

4. Each fuel exhibited a unique sensitivity to intake temperature, with the two high octane-sensitivity (S) fuels yielding similar KL-CA50 responses

5. The knock resistance of each fuel was derived via different "mechanisms;" varying degrees of thermal resistance, charge heating due to LTHR, and HoV charge cooling.

## Future Work

This study has investigated the relevance of RON and MON ratings at naturally aspirated and lightly boosted conditions using a compression ratio of 12:1. Future work will expand these experiments to encompass higher pressure and lower temperature compressed conditions enabled by a reduced compression ratio (10:1) and increased intake pressures.

## References


1. Heywood, J.B., Internal Combustion Engine Fundamentals, McGraw-Hill, New York, 1988.
2. Department of Energy, "Co-Optimization of Fuels & Engines." Department of Energy, Web. 12 Oct. 2016.
3. ASTM 2699, "Research Octane Number Test." 2016, www.astm.org/Standards/D2699
4. ASTM 2700, "Motor Octane Number Test." 2016, www.astm.org/Standards/D2700
5. Stein, Robert A., et al. "Effect of heat of vaporization, chemical octane, and sensitivity on knock limit for ethanol-gasoline blends." SAE International Journal of Fuels and Lubricants 5.2012-01-1277 (2012): 823-843.
6. Stein, Robert A., James E. Anderson, and Timothy J. Wallington. "An overview of the effects of ethanol-gasoline blends on SI engine performance, fuel efficiency, and emissions." SAE International Journal of Engines 6.2013-01-1635 (2013): 470-487.
7. Morganti, Kai, et al. Improving the Efficiency of Conventional Spark-Ignition Engines Using Octane-on-Demand Combustion. Part I: Engine Studies. No. 2016-01-0679. SAE Technical Paper, 2016.
8. Kalghatgi, G. T. Fuel anti-knock quality-Part I. Engine studies. No. 2001-01-3584. SAE Technical Paper, 2001.
9. Kalghatgi, Gautam T., Koichi Nakata, and Kazuhisa Mogi. Octane appetite studies in direct injection spark ignition (DISI) engines. No. 2005-01-0244. SAE Technical Paper, 2005.
10. Kalghatgi, Gautam, et al. Knock Prediction Using a Simple Model for Ignition Delay. No. 2016-01-0702. SAE Technical Paper, 2016.
11. Sluder, C. Scott, et al. "Exploring the Relationship Between Octane Sensitivity and Heat-of-Vaporization." SAE International Journal of Fuels and Lubricants 9.2016-01-0836 (2016): 80-90.
12. Zeng, W., Sjöberg, M., and Reuss, D., "Using PIV Measurements to Determine the Role of the In-Cylinder Flow Field for Stratified DISI Engine Combustion," SAE Int. J. Engines 7(2):615-632, 2014, doi:10.4271/2014-01-1237.
13. Sjöberg, M., Zeng, W., Singleton, D., Sanders, J. et al., "Combined Effects of Multi-Pulse Transient Plasma Ignition and Intake Heating on Lean Limits of Well-Mixed E85 DISI Engine Operation," SAE Int. J. Engines 7(4):1781-1801, 2014, doi:10.4271/2014-01-2615.
14. "Petroleum Products Research." SwRI Brochure. Southwest Research Institute, n.d. Web. 12 Oct. 2016.
15. Shahlari, A., Hocking, C., Kurtz, E. and Ghandhi, J., "Comparison of Compression Ignition Engine Noise Metrics in Low-Temperature Combustion Regimes," SAE Int. J. Engines 6(1):2013, doi:10.4271/2013-01-1659.
16. "Gamma Technologies | Engine and Vehicle Simulation." Gamma Technologies. Gamma Technologies, n.d. Web. 12 Oct. 2016.
17. Bradley, D., Morley, C., and Walmsley, H., "Relevance of Research and Motor Octane Numbers to the Prediction of Engine Autoignition," SAE Technical Paper 2004-01-1970, 2004, doi:10.4271/2004-01-1970.
18. CRC Performance Committee, "Coordinating Research Council Report No. 660," May 2011.
19. Mehl, M., et al. Detailed kinetic modeling of low-temperature heat release for PRF fuels in an HCCI engine. No. 2009-01-1806. SAE Technical Paper, 2009.
20. Sjöberg, Magnus, and John E. Dec. EGR and intake boost for managing HCCI low-temperature heat release over wide ranges of engine speed. No. 2007-01-0051. SAE Technical Paper, 2007.
21. Curran, Henry J., et al. "A comprehensive modeling study of n-heptane oxidation." Combustion and flame 114.1 (1998): 149-177.
22. Sarathy, S. Mani, et al. "Ignition of alkane-rich FACE gasoline fuels and their surrogate mixtures." Proceedings of the Combustion Institute 35.1 (2015): 249-257.
23. Vuilleumier, David, et al. Exploration of heat release in a homogeneous charge compression ignition engine with primary reference fuels. No. 2013-01-2622. SAE Technical Paper, 2013.
24. Mehl, Marco, et al. "An approach for formulating surrogates for gasoline with application toward a reduced surrogate mechanism for CFD engine modeling." Energy & Fuels 25.11 (2011): 5215-5223.
25. Vuilleumier, D., "The Effect of Ethanol Addition to Gasoline on Low- and Intermediate-Temperature Heat Release under Boosted Conditions in Kinetically Controlled Engines," Ph.D. Dissertation, Mechanical Engineering Department, University of California at Berkeley, 2016.


## Acknowledgments


The authors would like to thank Alberto Garcia, Gary Hubbard, Keith Penney, and Tim Gilbertson for their dedicated support of the DISI

laboratory. Benjamin Wolk and Gerald Gentz provided valuable input for the manuscript.

The work was performed at the Combustion Research Facility, Sandia National Laboratories, Livermore, CA. This research was conducted as part of the Co-Optimization of Fuels & Engines (Co-Optima) project sponsored by the U.S. Department of Energy (DOE) Office of Energy Efficiency and Renewable Energy (EERE), Bioenergy Technologies and Vehicle Technologies Offices. Sandia is a multi-mission laboratory operated by Sandia Corporation, a wholly owned subsidiary of Lockheed Martin Corporation, for the U.S. Department of Energy's National Nuclear Security Administration under contract DE-AC04-94AL85000.

## Definitions/Abbreviations

| | |
|---|---|
| **AHRR** | Apparent Heat Release Rate |
| **aTDC** | after Top Dead Center |
| **bTDC** | before Top Dead Center |
| **BOB** | Before Oxygenate Blendstock |
| **CA** | Crank Angles |
| **CAD** | Crank Angle Degrees |
| **CA30** | 30% Burn Point |
| **CA50** | 50% Burn Point |
| **CAI** | California Analytical Instruments |
| **CNL** | Combustion Noise Level |
| **CO** | Carbon Monoxide |
| **$CO_2$** | Carbon Dioxide |
| **Co-Optima** | Co-Optimization of Fuels and Engines |
| **CR** | Compression Ratio |
| **DHA** | Detailed Hydrocarbon Analysis |
| **DISI** | Directly-Injected Spark Ignition |
| **E30** | Gasoline blended with 30% by volume ethanol |
| **EGR** | Exhaust Gas Recirculation |
| **HC** | Hydrocarbon |
| **HoV** | Heat of Vaporization |
| **IMEP** | Indicated Mean Effective Pressure |
| **KI** | Knock Intensity |
| **KL-CA50** | Knock-Limited Combustion Phasing |
| **LTHR** | Low-Temperature Heat Release |
| **MBT** | Maximum Brake Torque |
| **MON** | Motor Octane Number |
| **NOx** | Nitrogen Oxide |
| **NTC** | Negative Temperature Coefficient |
| **$O_2$** | Oxygen |
| **OI** | Octane Index |
| **RON** | Research Octane Number |
| **SI** | Spark Ignition |
| **T10** | 10% Boiling Point Temperature |
| **T50** | 50% Boiling Point Temperature |
| **T90** | 90% Boiling Point Temperature |
| **TDC** | Top Dead Center |
| **TF** | Final Boiling Point Temperature |